Atmospheric Environment Vol. 24A, No. 9, pp. 2379–2386, 1990.
Printed in Great Britain.

0004–6981/90 $3.00 + 0.00
Pergamon Press plc

OVERALL EFFICIENCY OF TUBULAR INLETS SAMPLING AT 0–90 DEGREES FROM HORIZONTAL AEROSOL FLOWS

SUNIL HANGAL and KLAUS WILLEKE*
Aerosol Research Laboratory Department of Environmental Health University of Cincinnati, Cincinnati, OH 45267-0056, U.S.A.

(*First received* 2 *October* 1989 *and in final form* 1 *March* 1990)

Abstract—We have developed a unified and comprehensive model for the overall efficiency of tubular inlets sampling from horizontal aerosol flows at 0–90° relative to the wind direction. In our model, derived from experimental data obtained in our wind tunnel, the transmission efficiency is separated into two components: one due to gravitational settling in the boundary layer and the other due to impaction. The gravitational settling component is determined by extending our previously developed isoaxial sampling model to nonisoaxial sampling. The impaction component is determined by a new model that quantifies the particle losses caused by direct wall impaction. The model also quantifies the additional particle losses resulting from the turbulent motion in the vena contracta which is formed in the inlet when the inlet velocity is higher than the wind velocity.

The equation for the gravitational settling component considers the inertial behaviour of the particles by including the Stokes number, the flow development in the boundary layer by including the Reynolds number and the gravitational settling in the boundary layer by including a modified gravitational settling parameter. The equation for the impaction component considers direct wall impaction and the losses due to vena contracta formation through the Stokes number, velocity ratio and sampling angle. Direct wall impaction is further differentiated by the gravity effect on the impaction process which distinguishes upward from downward sampling. Our equations for transmission efficiency in combination with aspiration efficiency equations determine the overall efficiency of tubular, sharp-edged inlets at all orientations of the inlet relative to horizontal aerosol flows.

Key word index: Aerosol sampling, particle losses, inlet, aspiration efficiency, transmission efficiency, gravitational settling, wall impaction and vena contracta formation.

INTRODUCTION

Airborne particles are measured in ambient and industrial environments by drawing the particle-laden air through an opening to a direct reading sensor or collecting medium. It is essential that the sampled aerosol be representative of the aerosol in the free stream. The changes that occur during sampling must be assessed quantitatively so that the sampling errors can be compensated for. Figure 1 illustrates the processes that may change the aerosol concentration and size distribution during sampling: (1) aspiration to the face of the inlet; (2) bounce from the front edge of the inlet; (3) transmission loss in the inlet due to gravitational settling, direct wall impaction and turbulence in the vena contracta which is formed when the inlet velocity exceeds the ambient wind velocity.

The overall sampling efficiency, E_s, can thus be represented by the product of three distinct efficiencies:

$$E_s = E_a E_r E_t \tag{1}$$

where E_a is the aspiration efficiency, which is the ratio of particle concentration at the inlet face to the particle concentration in the undisturbed environment. E_r is the entry efficiency, which is the ratio of particle concentration passing the inlet face to the particle concentration incident to the face. E_t is the transmission efficiency, which is the ratio of particle concentration exiting the inlet to the particle concentration just past the inlet face.

Aspiration has been studied extensively (Belyaev and Levin, 1974; Durham and Lundgren, 1980; Jayasekara and Davies, 1980; Davies and Subari, 1982; Vincent *et al.*, 1986; Dunnett and Ingham, 1988; Rader and Marple, 1988; Liu *et al.*, 1989; Vincent, 1989). Equations for the aspiration efficiency, E_a, are presented further below.

For a sharp-edged inlet, particle bounce is negligible. Thus,

$$E_r = 1 \tag{2}$$

and Equation (1) reduces to

$$E_s = E_a E_t. \tag{3}$$

Experimental data on sampling efficiency have shown that for many sampling configurations most of the particle losses occur inside the inlet over the first 1 cm of the inlet (Tufto and Willeke, 1982). The losses in the inlet section cannot be explained by theories for fully

*To whom correspondence should be addressed.

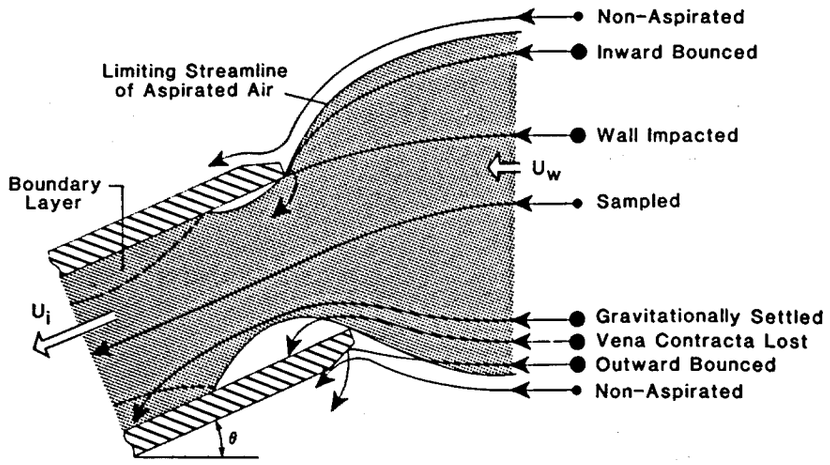

Fig. 1. Schematic representation of the mechanisms that affect the overall efficiency of a sampling inlet.

developed pipe flow (Okazaki and Willeke, 1987). This led to the development, in this laboratory, of a model for isoaxial sampling which quantifies the particle losses in the inlet as a function of gravitational settling in the developing boundary layer (Okazaki *et al.*, 1987a,b). In a study on the dominant mechanisms for sampling at 30–90°, aspiration was found to dominate up to about 45°, while impaction was found to dominate from about 45 to 90° (Okazaki *et al.*, 1987c).

We have now developed and will present here a unified and comprehensive model for the overall sampling efficiency of tubular inlets sampling from horizontal aerosol flows at 0–90°. In our model, derived from experimental data obtained in our wind tunnel, the transmission efficiency, E_t, is separated into two components: one due to gravitational settling, E_{ts}, and the other due to impaction, E_{ti}

$$E_t = E_{ts}\,E_{ti}. \tag{4}$$

The model for transmission efficiency due to gravitational settling that had previously been developed for isoaxial conditions has been extended from 0° to the entire range of 0–90°. A new model has been developed for the transmission efficiency due to impaction for the same range of 0–90°. This model quantifies the particle losses due to direct wall impaction as well as the additional particle losses due to turbulence in the vena contracta which is formed in the inlet when the inlet velocity exceeds the ambient wind velocity. Our transmission efficiency equations in combination with the aspiration efficiency equations determine the overall sampling efficiency of sharp-edged, tubular inlets sampling from horizontal aerosol flows at all orientations of the inlet relative to the wind direction.

EXPERIMENTAL DATA BASE

The development of our unified model has as a basis a large set of sampling efficiency data that has been obtained in our wind tunnel facility over several years (Tufto and Willeke, 1982a,b; Okazaki *et al.*, 1987a,b,c; Wiener *et al.*, 1988). In this wind tunnel facility monodisperse oleic acid particles, produced by a vibrating aerosol generator, are sampled in the test section by the inlet under study. The inlet is integrated into a modified optical single particle counter which permits fast data acqisition and analysis at high statistical counting efficiency for a wide range of inlet sizes and flow rates. Sampling efficiency data are available for tubular sharp-edged inlets of 20 cm length with internal diameters ranging from 0.32 to 1.59 cm (5/32–21/32 in). The particle size of the liquid aerosol ranges from 5 to 40 μm and the wind and inlet velocities from 125 to 1000 cm s^{-1}. The sampling angles are 0°, 15°, 30°, 60° and 90° upward or downward from the horizontal aerosol flow.

In the earlier work by Okazaki and Willeke (1987) and Okazaki *et al.* (1987c), the overall sampling efficiency, E_a, determined from wind tunnel experiments performed at sampling angles of 0–90°, was divided by the transmission efficiency, E_t, determined by wash-off techniques, which gave the aspiration efficiency data, E_a, that matched the Belyaev and Levin (1974) equation at 0° and the Laktionov (1973) equation at 90°. Therefore, we have taken all the E_a data and divided them by E_a to determine the transmission efficiencies for a wide range of conditions.

The Belyaev and Levin aspiration equation for isoaxial conditions is

$$E_a = 1+(R-1)\,(1-[1+(2+0.617/R)\,Stk]^{-1}) \tag{5}$$

where $R = U_w(U_i)^{-1}$ (6)

U_w = wind velocity, U_i = inlet velocity,

Stk = Stokes number $= \tau U_w(D_i)^{-1}$ (7)

τ = particle relaxation time $= \rho_p\, d_p^2\,(18\,\mu)^{-1}$ (8)

d_p = particle diameter, ρ_p = particle density and μ = air viscosity, D_i = inlet diameter.

The Laktionov equation for 90° is

$$E_a = 1-3\;Stk^{(R)^{-0.5}}. \tag{9}$$

For sampling from 0 to 90°, Durham and Lundgren (1980) developed the following empirical equation as a function of sampling angle θ.

$$E_a = 1+(R\cos\theta-1)\,(\beta(Stk', R))\,(\beta(Stk', R=1))^{-1}\,(\beta'(Stk')) \tag{10}$$

where $$Stk' = Stk\,\exp(0.022\,\theta) \tag{11}$$

$$\beta'(Stk') = 1-[1+0.55\,Stk'\,\exp(0.25\,Stk')]^{-1} \tag{12}$$

$$\beta(Stk', R) = 1-[1+(2+0.617/R)\,Stk']^{-1}. \tag{13}$$

The Durham and Lundgren equation is valid for $0.01 < Stk < 6$, and does not agree with the Laktionov equation at 90° for $R \neq 1$ (Durham and Lundgren, 1980). The Durham and Lundgren equation agrees with our experimental data on aspiration up to about 60°. We also found that it agrees with the Belyaev and Levin equation within the experimental error at isoaxial condition for all R. We have, therefore, extended the Laktionov eqution to include angles less than 90°

$$E_a = 1+(R\cos\theta-1)\,(3\;Stk^{(R)^{-0.5}}). \tag{14}$$

We found that Equation (14) agrees with our experimental data from about 45° to 90° within the Laktionov experimental range of $Stk = 0.003$–0.2. Therefore, we express aspiration efficiency by the Durham and Lundgren equation from 0 to 60° and the modified Laktionov equation from 45 to 90° (Hangal, 1990).

The transmission efficiency, E_t, for isoaxial sampling depends on the particle size, wind velocity and inlet velocity (Okazaki *et al.*, 1987a; Okazaki and Willeke, 1987). At non-isoaxial condition, the transmission efficiency is further influenced by the sampling angle. Figure 2 shows some of our transmission efficiencies, calculated from our overall sampling efficiency data through use of the aspiration efficiency equation by Durham and Lundgren for 0 to 60° and the Laktionov equation for 90°. As seen, the transmission efficiency declines with increase in sampling angle. For example, the transmission efficiency declines from 97% at 0° to 14% at 90° at $Stk = 0.2$ (aerodynamic particle diameter = 8.5 μm for a 5.7 mm inlet sampling at $U_w = U_i = 500$ cm s^{-1}).

MODEL DEVELOPMENT FOR TRANSMISSION EFFICIENCY

Transmission losses in the inlet are due to impaction and gravitational settling as illustrated in Fig. 1. The impaction component can be due to direct wall impaction as well as impaction on the wall through turbulence in the vena contracta. The vena contracta is formed when the inlet velocity is higher than the wind velocity (Mcabe and Smith, 1976). In the vena contracta secondary flows are formed which are turbulent. Particles are thrown against the wall through this turbulence and are lost due to impaction. Therefore, the transmission efficiency, E_t, can be separated into two components, one due to gravitational settling, E_{ts}, and the other due to impaction, E_{ti}, as shown earlier in Equation (4).

PARTICLE LOSSES DUE TO GRAVITATIONAL SETTLING

The loss of particles by gravitational settling is due to particle penetration into the boundary layer in the inlet and subsequent gravitational settling, as schematically shown in Fig. 3. We have modeled the gravitational settling component of the transmission efficiency by extending our model for isoaxial conditions (Okazaki and Willeke, 1987) to non-isoaxial conditions.

For isoaxial conditions, the following equation has been developed for transmission efficiency due to gravitational settling

$$E_t = \exp(-4.7\,K^{0.75}) \tag{15}$$

$$K = [(Stk\;Z)\;Re^{-0.5}]^{0.5}. \tag{16}$$

K is the parameter which expresses particle penetra-

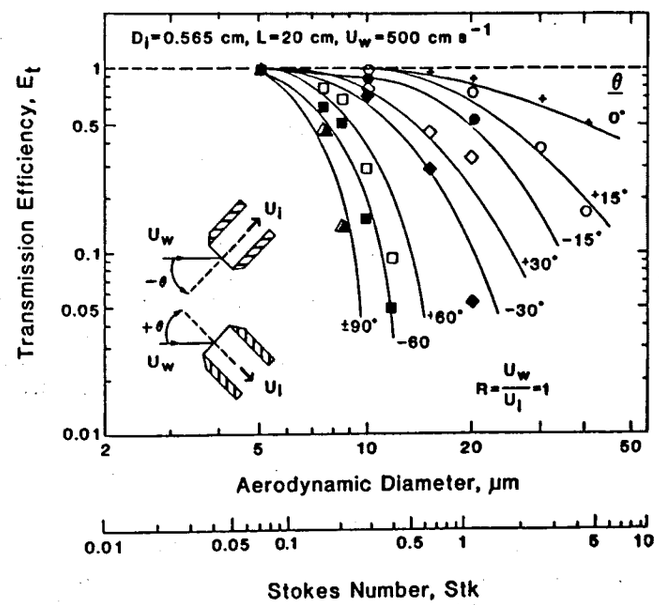

Fig. 2. The transmission efficiency from our experimental data at different sampling angles.

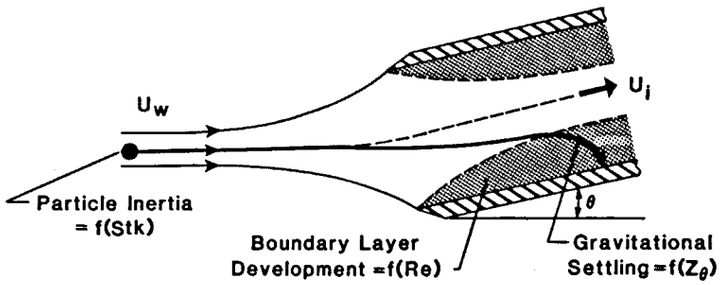

Fig. 3. Schematic representation of the gravitational settling mechanism in the inlet.

tion into the boundary layer and subsequent gravitational settling at isoaxial conditions. Stokes number, *Stk*, expresses the inertial penetration of the particles into the inlet. Reynolds number, Re, expresses the boundary layer development and gravitational settling parameter, Z, expresses the gravitational settling in the boundary layer, where V_s is the gravitational settling velocity.

$$Re = D_i U_i \rho (\mu)^{-1} \tag{17}$$

$$Z = (L/U_i)\,(D_i/V_s)^{-1} \tag{18}$$

where ρ = density of air, L = length of inlet

$$V_s = \text{settling velocity} = \tau g \tag{19}$$

where g = acceleration of gravity.

For non-isoaxial conditions, the pathway of the particle settling is determined by the settling velocity component, $V_s \cos\theta$. We have extended the model for isoaxial conditions to non-isoaxial conditions by inclusion of the angle effect:

$$Z_\theta = (L/U_i)\,(D_i/V_s \cos\theta)^{-1} = Z \cos\theta. \tag{20}$$

At non-isoaxial conditions, the boundary layer development and inertial penetration are expressed by the same Reynolds number and Stokes number, respectively. Therefore, the gravitational settling parameter at isoaxial conditions in equation (16) can be extended for all angles as,

$$K_\theta = [(Stk\, Z_\theta)\, Re^{-0.5}]^{0.5} = K(\cos\theta)^{0.5} \tag{21}$$

$$K_\theta = [d_p^2 \rho_p U_w L V_s \cos\theta\, (18\, D_i^{2.5}\, U_i^{1.5} \times (\rho\mu)^{0.5})^{-1}]^{0.5}. \tag{22}$$

The gravitational settling component, E_{ts}, of the transmission efficiency is thus, for all sampling angles:

$$E_{ts} = \exp(-4.7\, K_\theta^{0.75}). \tag{23}$$

The transmission efficiency data shown in Fig. 2 have thus been separated into the impaction and gravitational settling components as given by Equation (4) and shown in Fig. 4. The gravitational settling components for several sampling angles have been calculated from Equation (23). The impaction component have been determined by dividing the transmission efficiency data by the gravitational settling components. As seen, the gravitational settling component of transmission efficiency declines from unity at 90° (no gravitational losses) to its minimum at 0° and the impaction component declines from unity at 0° (no impaction losses) to its minimum at 90°.

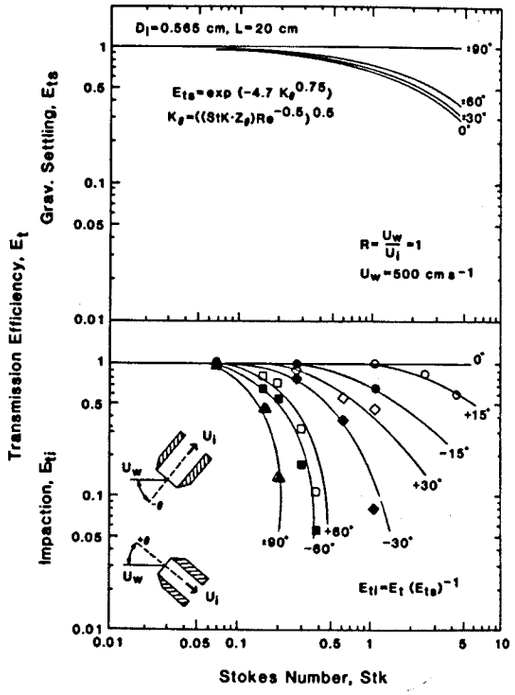

Fig. 4. The gravitational settling and impaction components of the transmission efficiency.

PARTICLE LOSSES DUE TO DIRECT WALL IMPACTION

When sampling at an angle, particles entering the inlet close to the wall may impact onto the wall. A particle's motion towards the inner wall is determined by the wind velocity component, $U_w \sin\theta$, and the gravitational settling component, $V_s \cos\theta$, as shown in Fig. 5. During upward sampling, the particles will impact onto the lower wall of the inlet. In this case, the wind and the gravitational settling velocity components act in the same direction, as shown in Fig. 5a. During downward sampling, the particles will impact onto the upper wall of the inlet with less inertia since the wind and gravitational settling velocity components oppose each other, as shown in Fig. 5b.

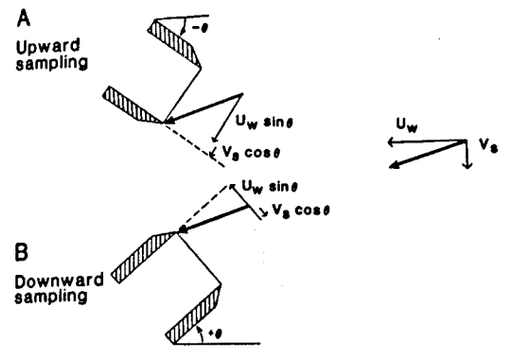

Fig. 5. The wind velocity and gravitational settling velocity components for upward and downward sampling.

Particles away from the wall and closer to the centerline will not impact onto the wall and will be carried downstream by the flow. A limiting condition separates impaction from no impaction, as illustrated in Fig. 6a. This limiting condition can be defined by the trajectory of the particle which impacts on the wall. All particles in the upper region impact onto the wall and all particles below this region are carried downstream. The depth of the impaction region is proportional to stopping distance, S, determined by wind velocity component $U_w \sin\theta$ and particle relaxation time τ

$$S = U_w \tau \sin\theta. \tag{24}$$

Gravity tends to pull the particle away from the wall during downward sampling. This decreases the depth of the impaction region, as shown in Fig. 6b. The stopping distance, S, is now proportional to the wind velocity component acting towards the wall, $U_w \sin\theta$, reduced by the gravitational settling velocity component, $V_s \cos\theta$, as shown in Fig. 6b. Therefore,

$$S = (U_w \sin\theta - V_s \cos\theta)\tau \tag{25}$$

$$S = U_w \sin(\theta - \alpha)\tau. \tag{26}$$

We have expressed the gravity effect on the impaction process by introducing the gravity effect angle α. This angle represents the decrease in actual angle θ that would yield the same stopping distance for wind vector U_w.

The fraction of particles impacting on the wall depends on the ratio of S to inlet diameter, D_i

$$S/D_i = U_w \tau \sin(\theta - \alpha)/D_i. \tag{27}$$

The fraction of particles entering the inlet that impacts directly onto the wall, I_w, is equal to the area of impaction over the cross-sectional area of the inlet, as

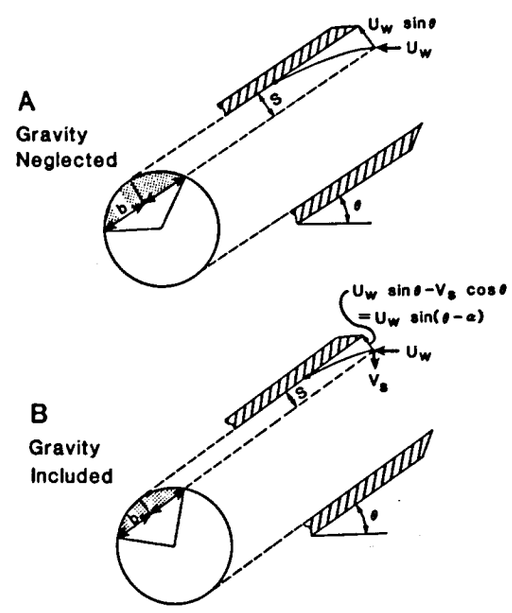

Fig. 6. The limiting trajectory for impaction and the impaction area during downward sampling. $R = 1$. (a) Effect of gravity neglected. (b) Included.

shown in Fig. 6. We have approximated the area of impaction by half the area of an ellipse with axes S and b,

$$I_w = 0.5 \Pi S\, b/(\Pi D_i^2/4). \tag{28}$$

Axis b is equal to the product of tube radius and the sine of half the angle covering the impaction sector. This angle is proportional to physical angle θ modified by gravity effect angle α. Since we are developing a non-dimensional number reflecting wall impaction, we neglect the proportionality coefficient

$$b = 0.5\, D_i \sin((\theta - \alpha)/2). \tag{29}$$

By combining Equations (28) and (29),

$$I_w = (S/D_i) \sin((\theta - \alpha)/2). \tag{30}$$

Substituting Equation (27) in Equation (30),

$$I_w = (\tau U_w/D_i) \sin(\theta - \alpha) \sin((\theta - \alpha)/2). \tag{31}$$

For upward sampling, the gravitational settling component and the wind velocity component both act towards the impaction wall, as shown earlier in Fig. 5a. Therefore, for upward sampling the impaction fraction is,

$$I_w = (\tau U_w/D_i) \sin(\theta + \alpha) \sin((\theta + \alpha)/2). \tag{32}$$

In general the wall impaction fraction is therefore

$$I_w = (\tau U_w/D_i) \sin(\theta \pm \alpha) \sin((\theta \pm \alpha)/2). \tag{33}$$

Equation (33) is valid for $R = 1$, i.e. the numerical values of wind and inlet velocity are equal to each other. When $R = 1$, a cylindrical fluid volume of diameter D_i enters the inlet, as shown in Fig. 7a. When

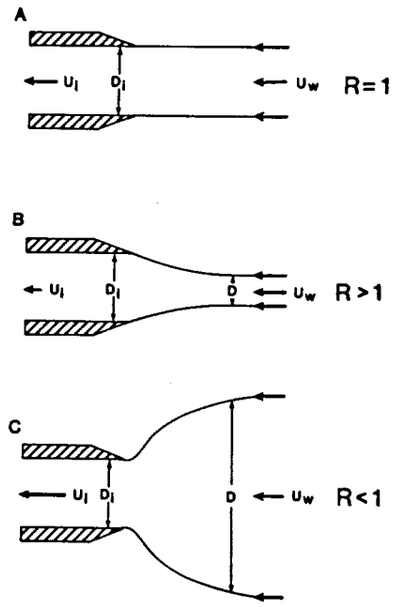

Fig. 7. The flow pattern during sampling.

$R \neq 1$, the diameter of the fluid volume, D, is smaller or larger than inlet diameter D_i, as shown in Figs 7b and 7c. By law of continuity,

$$D = D_i(U_i/U_w)^{0.5}. \quad (34)$$

The aerosol reaching the inlet face beyond which they may impact onto the inner wall depend on Stokes number expressed by fluid diameter D, which can be reexpressed in terms of the conventional Stokes number definition, Equation (7), relative to the inlet diameter D_i

$$\tau U_w/D_i = \tau U_w/(D_i(U_i/U_w)^{0.5}) = Stk(R)^{0.5} \quad (35)$$

Equation (33) is rewritten for all R,

$$I_w = Stk(R)^{0.5} \sin(\theta \pm \alpha) \sin((\theta \pm \alpha)/2). \quad (36)$$

Okazaki *et al.* (1987c) have shown that the overall sampling efficiency data at 90°, where impaction dominates over all other mechanisms, can be consolidated as a function of $Stk(R)^{0.5}$. Equation (36) for wall impaction has that same functional relationship.

The impaction component of the transmission efficiency, E_{ti}, is shown in Fig. 8 as a function I_w for all the experimental data. A best fit method was used to determine the value of the gravity effect angle, α. As seen in Fig. 8a, the wall impaction data for $R=1$ can be represented by a single curve as a function of I_w. For $R=2$, as seen in Fig. 8b, the data also fit the wall impaction curve. For $R=0.5$, however, the data at 15 and 30° are lower than the wall impaction curve. This is due to additional particle losses caused by the turbulence in the vena contracta which forms when $R<1$, as shown in Fig. 1. The difference between the data and the impaction curve, I_v, as shown in Fig. 8b,

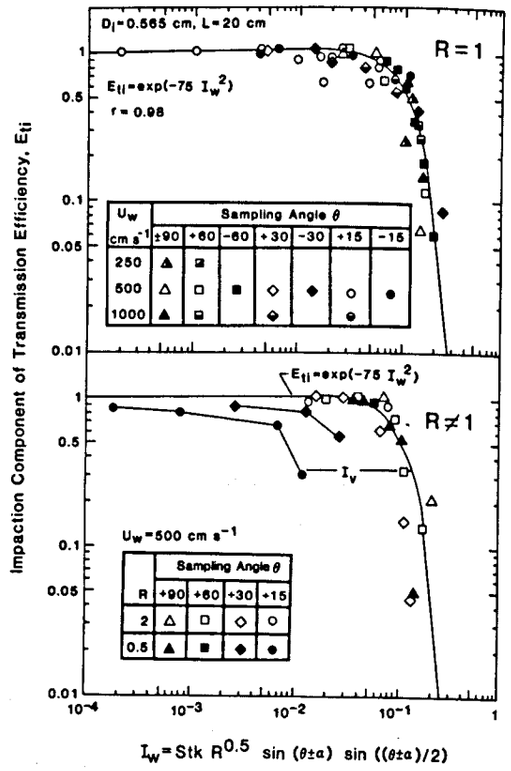

Fig. 8. The impaction component of the transmission efficiency as a function of direct wall impaction parameter, I_w. I_v represents the additional losses in the vena contracta due to turbulence when $R<1$.

represents the particles impacted on the wall due to vena contracta turbulence. By means of a best fit method the two types of impaction have been combined so that the impaction component of the transmission efficiency is now,

$$E_{ti} = \exp[-75(I_w + I_v)^2] \quad (37)$$

where I_w is the direct wall impaction parameter determined by Equation (36) and I_v is the vena contracta impaction parameter. I_v is zero for $R \geq 1$.

A best fit method has been used to determine the relationship between gravity effect angle, α, and physical sampling angle, θ,

$$\alpha = 12[(1 - \theta/90) - \exp(-\theta)]. \quad (38)$$

As shown in Fig. 9, α peaks at a 5° sampling angle but is highly dependent on the 15° data point. This indicates that the difference between downward and upward sampling reaches a maximum somewhere between 5 and 15°.

PARTICLE LOSSES DUE TO TURBULENCE IN THE VENA CONTRACTA

The fraction of particles that has entered the inlet and has been impacted onto the inner wall due to the turbulence in the vena contracta is proportional to the amount of turbulent flow in the vena contracta, V, and the removal efficiency of particles in the vena contracta, η. The flow in the vena contracta is proportional to the extra flow that is contracted into the inlet when $R<1$ as shown in Fig. 10a.

$$V \propto (A_o - A_i) A_o^{-1} \propto 1 - (A_i/A_o)$$
$$\propto 1 - (U_w/U_i) \propto 1 - R \quad (39)$$

where A_o is the cross-sectional area of the external flow that contracts into the cross-sectional area of the inlet, A_i.

At non-isoaxial conditions, the projected area of the inlet decreases by a $\cos\theta$ factor as illustrated in Fig. 10b. Therefore, the flow that is in the vena contracta also decreases by a factor proportional to $\cos\theta$

$$V \propto (1 - R)\cos\theta. \quad (40)$$

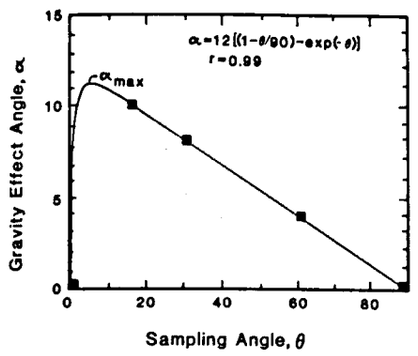

Fig. 9. Dependence of gravity effect angle, α, on physical sampling angle, θ.

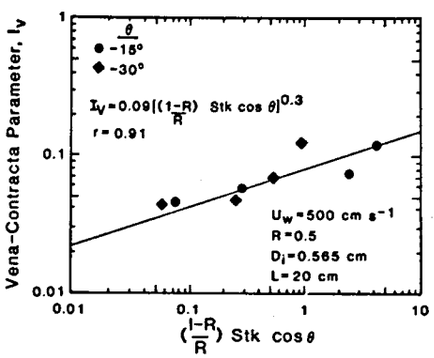

Fig. 11. Dependence of vena contracta parameter, I_v, on Stokes number, sampling angle and velocity ratio.

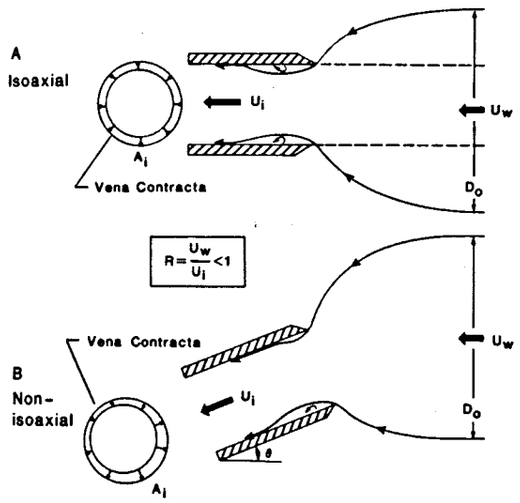

Fig. 10. Vena contracta formation. (a) Isoaxial condition. (b) Non-isoaxial condition.

The removal efficiency of particles in the vena contracta, η, depends on the ratio of particle stopping distance, S, to inlet diameter, D_i

$$\eta = S(D_i)^{-1} = \tau U_i(D_i)^{-1}. \quad (41)$$

The stopping distance is proportional to the impaction velocity of the particles which is assumed to be equal to the inlet velocity, U_i. Equation (41) can thus be rewritten as

$$\eta = (\tau U_w D_i^{-1})(U_i U_w^{-1}) = Stk(R)^{-1}. \quad (42)$$

The fraction of particles lost due to impaction in the vena contracta, I_v, is given by combining Equations (40) and (42)

$$I_v \propto \eta V \propto (1 - R) R^{-1} Stk\cos\theta. \quad (43)$$

The values of impaction parameter, I_v, from Fig. 8 are shown in Fig. 11. All the data are represented by a single curve determined by a best fit method

$$I_v = 0.09[(1 - R) R^{-1} Stk\cos\theta]^{0.3}. \quad (44)$$

SUMMARY OF RELEVANT EQUATIONS

In order to facilitate the use of these data-based models the equations that determine the overall efficiency of inlets sampling from horizontal aerosol flows are summarized as follows: The overall sampling efficiency, E_s, is a product of aspiration efficiency, E_a, entry efficiency, E_r, and transmission efficiency, E_t

$$E_s = E_a E_r E_t. \quad (1)$$

For sharp-edged inlets, $E_r = 1$ and E_s reduces to

$$E_s = E_a E_t. \quad (3)$$

The transmission efficiency is further separated into gravitational settling component, E_{ts}, and impaction component, E_{ti}

$$E_t = E_{ts} E_{ti}. \quad (4)$$

The individual components of the overall sampling

efficiency have been expressed as shown below. All depend on the Stokes number, Stk, and velocity ratio, R, defined as

$$Stk=\tau U_w(D_i)^{-1} \quad (7)$$

$$R=U_w(U_i)^{-1}. \quad (6)$$

(a) Aspiration efficiency, E_a:
for $0\leqslant\theta\leqslant 60°$

$$E_a=1+[R\cos\theta-1][1-(1+(2+0.617/R)\,Stk')^{-1}][1-(1+2.617\,Stk')^{-1}]^{-1}$$

$$[1-(1+0.55\,Stk'\exp(0.25\,Stk'))^{-1}] \quad (10)$$

$$Stk'=Stk\exp(0.022\,\theta). \quad (11)$$

For $45\leqslant\theta\leqslant 90°$,

$$E_a=1+(R\cos\theta-1)(3\,Stk^{(R)^{-0.5}}). \quad (14)$$

(b) Gravitational component of the transmission efficiency, E_{ts}:

$$E_{ts}=\exp(-4.7\,K_\theta^{0.75}) \quad (23)$$

$$K_\theta=[(Stk\,Z_\theta)\,Re^{-0.5}]^{0.5} \quad (21)$$

$$Re=D_iU_i\rho(\mu)^{-1} \quad (17)$$

$$Z_\theta=(L/D_i)(V_s\cos\theta/U_i). \quad (20)$$

(c) Impaction component of the transmission efficiency, E_{ti}:

$$E_{ti}=\exp[-75(I_w+I_v)^2] \quad (37)$$

$$I_w=Stk\,R^{0.5}\sin(\theta\pm\alpha)\sin((\theta\pm\alpha)/2) \quad (36)$$

$$\alpha=12[(1-\theta/90)-\exp(-\theta)] \quad (38)$$

$$I_v=0.09[(1-R)\,R^{-1}\,Stk\cos\theta]^{0.3} \text{ for } R<1 \quad (44)$$

$$I_v=0 \text{ for } R\geqslant 1.$$

SAMPLE CALCULATIONS

Given: $D_i=5.7$ mm, $L=20$ cm, $\theta=\pm 30$,

$U_w=250$ cm s^{-1}, $U_i=500$ cm s^{-1},

d_{ae} = aerodynamic particle diameter $=20\ \mu$m.

(a) Aspiration efficiency: $E_a=0.74$.

(b) Gravitational component of the transmission efficiency:

$$E_{ts}=0.71.$$

(c) Impaction component of the transmission efficiency:

$$E_{ti}(\text{downward})=0.49$$

$$E_{ti}(\text{upward})=0.20.$$

(d) Overall sampling efficiency:

$$E_a(\text{downward})=0.74\times 0.71\times 0.49=0.26$$

$$E_a(\text{upward})=0.74\times 0.71\times 0.20=0.10.$$

Acknowledgement—Sunil Hangal was financially supported for his Ph. D. study by a graduate research assistantship from the University of Cincinnati.

REFERENCES

Belyaev S. P. and Levin L. M. (1974) Techniques for collection of representative aerosol samples. *J. Aerosol Sci.* **5**, 325–338.

Davies C. N. and Subari M. B. (1982) Aspiration above wind velocity of aerosols with thin walled nozzles facing and at right angles to the wind direction. *J. Aerosol Sci.* **13**, 59–71.

Durham M. D. and Lundgren D. A. (1980) Evaluation of aerosol aspiration efficiency as a function of Stokes number, velocity ratio and nozzle angle. *J. Aerosol Sci.* **11**, 179–188.

Dunnett S. J. and Ingham D. B. (1988) An empirical model for the aspiration efficiencies of blunt aerosol samplers oriented at an angle to the oncoming flow. *Aerosol Sci. Technol.* **8**, 245–264.

Hangal S. (1990) Comprehensive modeling of the overall efficiency of sampling inlets. Ph.D. Thesis, University of Cincinnati, Cincinnati, Ohio, U.S.A.

Jayasekara P. N. and Davies C. N. (1980) Aspiration below the wind velocity of aerosols with sharp edged nozzles facing the wind. *J. Aerosol Sci.* **11**, 535–547.

Laktionov A. B. (1973) Aspiration of an aerosol into a vertical tube from a flow transverse to it. *Fizika Aerozoley* **7**, 83–87 (Translation from Russian: AD-760 947, Foreign Technology Division, Wright-Patterson Air Force Base, Dayton, OH, U.S.A.).

Liu B. Y. H., Zhang Z. Q. and Keun T. H. (1989) A numerical study of inertial errors in anisokinetic sampling. *J. Aerosol Sci.* **20**, 367–380.

Mcabe W. L. and Smith J. C. (1976) *Unit Operations in Chemical Engineering*, Third Edition, chapter 3. McGraw Hill, New York.

Okazaki K., Wiener R. W. and Willeke K. (1987a) Isoaxial sampling: nondimensional representation of overall sampling efficiency. *Envir. Sci. Technol.* **21**, 178–182.

Okazaki K., Wiener R. W. and Willeke K. (1987b) The combined effect of aspiration and transmission on aerosol sampling accuracy for horizontal isoaxial sampling. *Atmospheric Environment* **21**, 1181–1185.

Okazaki K., Wiener R. W. and Willeke K. (1987C) Non-isoaxial aerosol sampling: mechanisms controlling the overall sampling efficiency. *Envir. Sci. Technol.* **21**, 183–187.

Okazaki K. and Willeke K. (1987) Transmission and deposition behavior of aerosols in sampling inlets. *Aerosol Sci. Technol.* **7**, 275–283.

Rader D. J. and Marple V. A. (1988) A study of the effects of anisokinetic sampling. *Aerosol Sci. Technol.* **8**, 283–299.

Tufto P. A. and Willeke K. (1982a) Dependence of particulate sampling efficiency on inlet orientation and flow velocity. *Am. Ind. Hyg. Ass. J.* **43**, 436–442.

Tufto P. A. and Willeke K. (1982b) Dynamic evaluation of aerosol sampling inlets. *Envir. Sci. Technol.* **16**, 607–609.

Vincent J. H. (1989) *Aerosol Sampling Science and Practice*, chapter 6. John Wiley, New York.

Vincent J. H., Stevens D. C., Mark D., Marshall M. and Smith T. A. (1986) On the aspiration characteristics of large diameter, thin-walled aerosol sampling probes at yaw orientation with respect to the wind. *J. Aerosol Sci.* **17**, 211–224.

Wiener R. W., Okazaki K. and Willeke K. (1988) Influence of turbulence on aerosol sampling efficiency. *Atmospheric Environment* **22**, 917–928.

Atmospheric Environment Vol. 24A, No. 9, pp. 2387–2395, 1990.
Printed in Great Britain.

0004-6981/90 $3.00+0.00
Pergamon Press plc

A STATISTICAL PROCEDURE FOR DETERMINING THE BEST PERFORMING AIR QUALITY SIMULATION MODEL

WILLIAM M. COX and JOSEPH A. TIKVART
United States Environmental Protection Agency, Office of Air Quality Planning and Standards (MD-14), Research Triangle Park, NC 27711, U.S.A.

(*First received* 19 *September* 1989 *and in final form* 21 *February* 1990)

Abstract—Air quality simulation models have been the subject of extensive evaluations to determine their performance under a variety of environmental and meteorological conditions. While much information has been gathered, no clearly defined methodology exists for comparing the performance of two or more models. The purpose of this paper is to present a statistically oriented procedure to test if the performance of one model is superior to others using a composite performance index involving the bootstrap resampling technique.

Key word index: Air quality models, model performance, model comparisons, statistical analysis, bootstrap resampling.

1. BACKGROUND AND PURPOSE

EPA has conducted an extensive program to evaluate the performance of air quality simulation models used for regulatory purposes (Cox and Tikvart, 1985). The statistical foundation for evaluating models was established as the result of two workshops sponsored jointly by EPA and the American Meteorological Society and summarized by Fox (1981, 1984). Based on recommendations from these workshops, EPA set out to develop a comprehensive library of statistics that summarizes the performance of various model categories. While this goal has been achieved (e.g. Londergan *et al.*, 1982; EPA, 1985, 1986, 1987), the resulting array of statistics are so diverse and numerous that it is difficult to objectively compare the overall performance of competing models (EPA, 1984).

Since completion of the original model evaluation studies, advances have been made in statistical methodology for calculating uncertainty that require fewer assumptions about the form of the underlying probability distribution (Efron, 1982). Using this newer methodology, it is now feasible to aggregate model evaluation results from various averaging periods and from different meteorological regimes and to compare aggregated results for different models in a probabilistic framework. In addition, statistical methodologies have been developed (Brieman *et al.*, 1979) and applied (Rao *et al.*, 1985) that allow treatment of extreme concentrations in the context of model evaluation. Concentrations from the upper end of the distribution are of great concern to regulators because of the nature of many existing air quality standards.

The purpose of this paper is to describe a method for aggregating component results of model performance into a single performance measure that may be used to compare the overall performance of two or more models. The distribution of the difference in composite performance between models is determined by using the bootstrap resampling technique (Efron, 1982). Results from different data bases are combined using a technique related to meta-analysis to produce an overall result. An example of the method is provided in which the performance of two rural models is compared using SO_2 data collected around four large midwestern power plants.

2. METHODOLOGY

The methodology is derived from EPA's experience in evaluation of isolated rural point source models located in essentially flat terrain. A strong emphasis is placed on the ability of models to predict peak concentrations independent of time of occurrence for two primary reasons: (1) the inherent limitations of most model evaluation data bases and (2) the specific regulatory purposes for which models are used. A major limitation of data commonly used to evaluate point source models is the lack of accurate information necessary to pinpoint actual transport wind direction. Data bases for rural models are usually rich in terms of the number of observations (time periods) but relatively sparse in terms of the size of the monitoring network. This fact argues for using peak concentrations under the assumption that "the data are dense enough in time to define the maximum concentration for each stability class at each of the monitors" (Irwin and Smith, 1984).

The other reason for focusing on peak concentrations is that rural models are used to estimate the impact of sources on ambient standards or increments. Because of the nature of some ambient stan-